Phys Chem Minerals (2007) 34:73–84
DOI 10.1007/s00269-006-0129-3

ORIGINAL PAPER

Basal slip and texture development in calcite: new results from torsion experiments

D. J. Barber · H.-R. Wenk · J. Gomez-Barreiro · E. Rybacki · G. Dresen

Received: 11 April 2006 / Accepted: 18 October 2006 / Published online: 14 December 2006

Abstract The deformation behavior of calcite has been of longstanding interest. Through experiments on single crystals, deformation mechanisms were established such as mechanical twinning on $\mathbf{e} = \{\bar{1}018\}\langle 40\bar{4}1\rangle$ in the positive sense and slip on $\mathbf{r} = \{10\bar{1}4\}\langle 20\bar{2}\bar{1}\rangle$ and $\mathbf{f} = \{\bar{1}012\}\langle 0\bar{2}2\bar{1}\rangle$, both in the negative sense. More recently it was observed that at higher temperatures $\mathbf{f}\{\bar{1}012\}\langle 10\bar{1}1\rangle$ slip in both senses becomes active and, based on slip line analysis, it was suggested that $\mathbf{c}(0001)\langle 11\bar{2}0\rangle$ slip may occur. So far there had been no direct evidence for basal slip, which is the dominant system in dolomite. With new torsion experiments on calcite single crystals at 900 K and transmission electron microscopy, this study identifies $(0001)\langle 11\bar{2}0\rangle$ slip unambiguously by direct imaging of dislocations and diffraction contrast analysis. Including this slip system in polycrystal plasticity simulations, enigmatic texture patterns observed in compression and torsion of calcite rocks at high temperature can now be explained, resolving a long-standing puzzle.

D. J. Barber
Physics Centre, University of Essex,
Colchester CO4 3SQ, UK

D. J. Barber
Wolfson Centre for Materials Processing,
Brunel University, Uxbridge UB8 3PH, UK

H.-R.Wenk (✉) · J. Gomez-Barreiro
Department of Earth and Planetary Science,
University of California, Berkeley, CA 94720, USA
e-mail: wenk@berkeley.edu

E. Rybacki · G. Dresen
GeoForschungsZentrum, Telegrafenberg,
14473 Potsdam, Germany

Keywords Calcite · Torsion experiments · Texture · Basal slip · TEM

Introduction

Calcite has long been at the center of experimental mineral deformation studies. Pioneering investigations on single crystals established mechanical twinning (Dove 1860; Baumhauer 1879); experiments by Muegge (1898) and Johnsen (1902) were attempts to document translation gliding. Deformation experiments on marble illustrated complex microstructures in polycrystals (Adams and Nicolson 1901). More than 50 years later deformation of calcite crystals and calcite rocks was again approached with modern apparatus at high pressure and temperature, resulting in the classical Yule marble studies (e.g., Griggs et al. 1953; Turner et al. 1954). Microstructures, investigated with the petrographic microscope, and development of preferred orientation patterns were interpreted in terms of microscopic deformation mechanisms such as slip and mechanical twinning (e.g., Turner et al. 1956). In these experiments, at up to 800 K, the relative importance of twinning on $\mathbf{e}\{\bar{1}018\}\langle 40\bar{4}1\rangle$, slip on $\mathbf{r}\{10\bar{1}4\}\langle 20\bar{2}\bar{1}\rangle$ and $\mathbf{f}\{\bar{1}012\}\langle 10\bar{1}1\rangle$ was established. Based on these mechanisms, fabrics in naturally deformed carbonate rocks were interpreted in terms of paleostress (e.g., Jamison and Spang 1976; Lacombe and Laurent 1992; Rowe and Rutter 1990) and deformation history (e.g., Burlini et al. 1998; Dietrich and Song 1984; Erskine et al. 1993; Ratschbacher et al. 1991; Schmid et al. 1981).

Deformation experiments on carbonate rocks at higher temperature illustrated pronounced changes in

preferred orientation patterns in compression (Wenk et al. 1973) as well as under plane strain (Barnhoorn et al. 2004; Kern and Wenk 1983; Pieri et al. 2001b; Rutter et al. 1994; Schmid et al. 1987; Wagner et al. 1982). These patterns were difficult to reconcile with the known deformation mechanisms (Wenk et al. 1986). Since then a comprehensive study of calcite single crystals at temperatures from 600 K to 1,100 K was conducted by De Bresser and Spiers (1997) and led to a new assessment of slip and, based on slip line analysis, it was suggested that $\mathbf{c}(0001)\langle 11\bar{2}0\rangle$ is an additional slip system in calcite. Above 700 K, $\mathbf{f}\{\bar{1}012\}\langle 0\bar{2}2\bar{1}\rangle$ slip is replaced by $\mathbf{f}\{\bar{1}012\}\langle 10\bar{1}1\rangle$ slip. So far there has been no direct evidence for basal slip dislocations. Activation of basal slip in single crystal compression experiments is limited because, for most orientations, other slip systems are strongly activated.

In this investigation we are approaching basal slip from two angles: First, we deform a single crystal of calcite in simple shear under the same conditions as the rock but in an orientation that is only conducive for basal slip and then investigate dislocations by transmission electron microscopy. Second, we investigate textures in fine-grained calcite rocks deformed in torsion at high temperature to large strains and then we interpret the experimental textures by comparing them with simulations based on polycrystal plasticity theory, assuming different slip system activities. In summary, the evidence largely confirms the suggestions of De Bresser and Spiers (1997) and establishes basal $\langle a\rangle$ slip as an important slip system of calcite at high temperature. Furthermore we document activity of rhombohedral $\langle a\rangle$ slip that is significant for interpreting recrystallization textures.

Torsion experiment on calcite single crystal

Torsion experiments on single crystals have the advantage that by choosing special orientations single slip systems can be activated, which is often not possible in compression of crystals with many potential slip systems. This method has already been applied by Borg and Handin (1967) to search for potential as-yet-undiscovered slip systems in calcite. These room temperature experiments could only confirm the previously known systems, twinning on $\mathbf{e} = \{\bar{1}018\}\langle 40\bar{4}1\rangle$ in the positive sense, slip on $\mathbf{r} = \{10\bar{1}4\}\langle 20\bar{2}1\rangle$ and $\mathbf{f} = \{\bar{1}012\}\langle 0\bar{2}2\bar{1}\rangle$, both in the negative sense.

In the search for **c**-slip we chose a calcite from South Africa and cored it parallel to the c-axis to produce a cylinder with a diameter of 10 mm and a length of 8.7 mm. In this geometry the potential (basal) slip plane is parallel to the shear plane and no other slip systems should be activated at low strain. The sample was jacketed using a steel sleeve and twisted in a Paterson-type rock deformation apparatus at 400 MPa confining pressure and 900 K temperature. Deformation was carried out at constant twist rate of 5×10^{-4} s^{-1}, corresponding to a shear strain rate of 2.9×10^{-4} s^{-1} at the sample periphery. The measured torque was corrected for apparatus compliance and jacket strength and converted to shear stress at the outer sample surface following the procedures described by Paterson and Olgaard (2000) and Rybacki et al. (2003), assuming a power law rheology with a stress exponent of 4.5. Accuracy of stress is about 4%, of strain ≈1%, and of temperature ≈0.3%, owing to precision of sensors and conversion procedures. Twisting was terminated after a small shear strain γ of about 0.04. After yielding at $\gamma \approx 0.01$ a constant shear stress of about 26 MPa at the sample periphery was sustained. The torque was maintained constant during cooling at a rate of 30°C min^{-1} to allow for microstructural investigations.

Transmission electron microscopy

Thin slices were cut from the outer part of the deformed single crystal, parallel to the $\mathbf{a} = \{11\bar{2}0\}-$ and $\mathbf{m} = \{10\bar{1}0\}-$ planes, respectively, utilizing a set of visible $\{10\bar{1}4\}$cleavage planes (some fracturing). The **m**- section contains traces of the potential **c**-slip planes and $\langle 11\bar{2}0\rangle$ slip directions. Two argon ion-milled specimens were made from the **a**-slices and one from an **m**-slice. Milling was performed at 5 kV, 0.8 mA and 11°. A JEOL 200-CX transmission electron microscope (TEM) was used, operated at 200 kV and equipped with a double-tilt stage.

Damage by the electron beam is a problem with calcite, but experience has shown that the rate of damage depends on: (a) the source of the sample, i.e., the impurity content; (b) the thermal history (the rate is generally lower in specimens that have recently been subject to high temperature). The twisted calcite was found to suffer damage at a fairly low rate. The determination of Burgers vectors, **b**, of dislocations by TEM requires the acquisition of at least three images under different ''two-beam'' diffraction conditions, in order to apply the $\mathbf{g}.\mathbf{b} = 0$ and $\mathbf{g}.\mathbf{b}\wedge\mathbf{u} = 0$ 'invisibility' criteria (Hirsch et al. 1965), where **g** is the diffraction vector and **u** is the direction vector of the dislocation. Specimens were placed in the double-tilt stage with important crystallographic directions set parallel to the axes of tilt. Minimum exposure was achieved by setting up diffraction conditions and focusing on a part of the

crystal adjacent to the area of choice. Final adjustments were then made quickly, prior to a single exposure. Thus it was possible to acquire sufficient images without excessive damage being apparent in the last image obtained. Pairs of images for viewing the dislocations stereoscopically were obtained by tilting through suitable angles while retaining the same main diffraction vector.

The deformation of the single crystal sample was somewhat non-uniform, as could be deduced from inspection by optical microscopy. Parts of the drum showed considerable amounts of fracture, mostly in the form of short cleavage cracks. Some deformation twinning on the **e**-planes $\{\bar{1}018\}$ was also present. At first sight there was little TEM evidence of basal slip in either of the **a**-sections. The **m**-section, however, was immediately recognized as appearing very different from most deformed calcites, which typically contain irregular dislocation arrangements, often forming loose networks. Instead, regions of the **m**-section exhibited parallel sets of long, rather straight dislocations that appear to be serrated. Examples can be seen in Fig. 1. Trace analysis based on electron diffraction patterns showed that the dislocations lie parallel to a $\langle\bar{2}110\rangle$ direction. Closer inspection of the ''serrations'' by tilting reveals that some of the dislocations are, in fact, slightly helical, a characteristic that is found in metals when a screw dislocation is affected by climb (e.g., Barrett and Massalski 1980, p 395). Indeed, these basal screws in calcite appear very similar to those seen in dolomite when the $(0001)\langle\bar{2}110\rangle$ system operates (cf. Fig. 7c, Barber et al. 1981).

Tilting was carried out to achieve imaging under suitable two-beam conditions for determination of the Burgers vectors of the dislocations. Assigning the direction of the long dislocations the axis $[\bar{2}110]$, the dislocations are in strong contrast for the reflections $\bar{1}104, 11\bar{2}0$ and show only weak contrast when imaged with $01\bar{1}8, 0006$ and other allowed $000l$ reflections. This is illustrated in Fig. 2. The diffraction contrast behavior proves that the Burgers vectors of the dislocation are parallel to $[\bar{2}110]$, i.e., they are screw dislocations. Note that in the dark field image, Fig. 2d, the ''out-of-contrast'' dislocations are given greater visibility by their accumulating clusters of point defects induced by the electron beam.

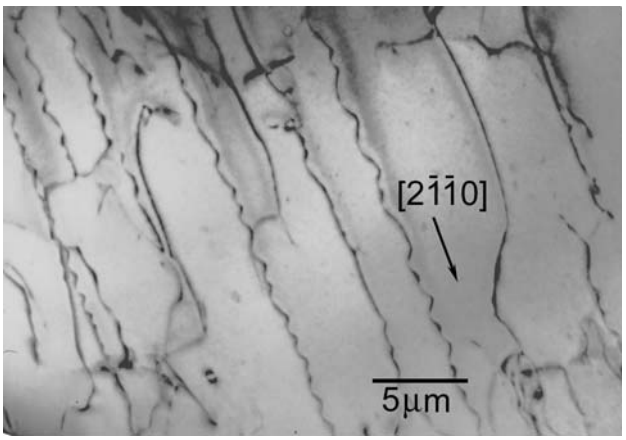

Fig. 1 TEM image of screw dislocations in calcite produced by basal slip and seen when viewed along an m-axis. The small serrations indicate the action of climb; the larger offsets are probably due to cross-slip

Stereoscopic pairs of images, coupled with comparison of projected image widths, enabled us to determine which dislocations lay in basal planes and which involved other slip planes. For this purpose it was necessary to tilt using a thick region of the specimen, necessitating fairly long exposures. The resulting negatives were not ideal and it has been necessary to improve and balance the contrast of the images by means of digital processing. Figure 3 is a stereo pair from a set of images of dislocations, mostly with $\langle a\rangle$ Burgers vectors, which established that some groups of dislocations (e.g., arrows, P) lie in the basal plane. This is apparent because images (a) and (b) are recorded on the same side of the $\langle 10\bar{1}0\rangle$ axis (and **c**-plane) whereas image (c) is from the opposite side. The sense of inclination of the short dislocations (basal edges) has reversed in image (c). Loose tangles (regions Q' and Q'') lie in an **r**-plane. Basal screws (largely uninteracted near P) feature prominently in these tangles, which implies that they have moved onto the **r**-plane by cross-slip.

Both **c**-slip $(0001)\langle\bar{2}110\rangle$ and **r**-slip $\{10\bar{1}4\}\langle 20\bar{2}\bar{1}\rangle$ have been activated in some volumes of the specimen, together with twinning on the **e**-planes and cleavage fracturing. In these regions the dislocation arrangements are generally more complicated than for those generated mainly by basal slip; many occur as components of loose irregular networks that were imaged and examined stereoscopically. Within these networks, segments of dislocation with Burgers vectors parallel to $\langle\bar{2}110\rangle$ have been identified by the two-beam diffraction contrast experiments, as illustrated by two images in Fig. 4 (note the segments that are arrowed). This figure also illustrates how the effect of damage to the crystal structure causes the **r**-slip plane that has been active to become visible. Similar damage is likely where dislocations have traversed the basal planes but it is not readily imaged as these planes are closely parallel to the electron beam when working with the **m**-section.

A further indication that the networks form as a result of cross-slip is the occurrence of basal screws that are neither straight nor helical, but are zig-zagged.

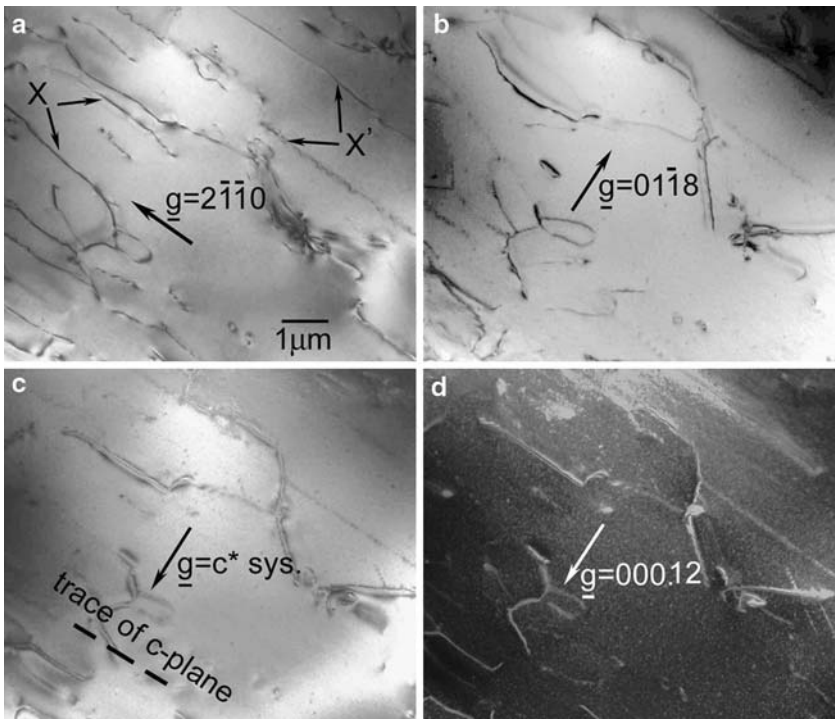

Fig. 2 TEM images from tilt experiments which show that the long dislocations have Burgers vectors parallel to the [$\bar{2}$110] direction. The dislocations do not become completely invisible when the diffraction vector **g** is parallel to the Burgers vector, **b**, because of elastic anisotropy and the effects of radiation damage

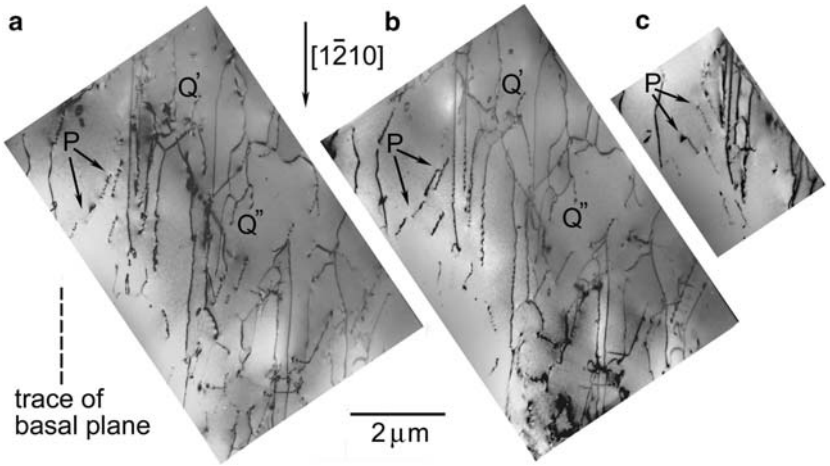

Fig. 3 Stereoscopic TEM images **a**, **b** of more long $\langle 11\bar{2}0 \rangle$ screw dislocations, proving that they lie in the basal planes. The images **a** and **b** were recorded when the specimen was tilted on one side of the m-axis while **c** was recorded on the opposite side. The change in the sense of tilt of the short dislocations at *P* shows that they are edge dislocations lying in the basal planes

This characteristic of some of the dislocations is not apparent unless they are viewed from more than one direction. The zig-zagging is apparently caused by cross-slip into a rhombohedral plane and is shown in Fig. 5. A central part of the screw dislocation viewed from off an m-axis in Fig. 5a is seen to have moved onto an **r**-plane when the specimen is tilted about an axis parallel to the screw to bring the electron beam parallel to the m-axis, in Fig. 5b.

The determination of the Burgers vectors of dislocations using the 'invisibility' criteria, $\mathbf{g}.\mathbf{b} = 0$ and $\mathbf{g}.\mathbf{b}\wedge\mathbf{u} = 0$ (Hirsch et al. 1965), developed for cubic materials, does work with carbonates, although dislocations do not generally become completely invisible, but instead show weak contrast. This residual contrast is least when the dislocation lies in a plane of high symmetry. Another factor that prevents dislocations becoming invisible is the accumulation of point defects in the dislocation cores as a result of electron beam damage. Thus they become ''decorated''. Moreover the paths that dislocations have traversed also accumulate damage, which provides a very convenient means of identification of the activated slip planes. This effect can be seen in Fig. 4.

The images obtained show that the long, slightly helical dislocations, which lie parallel to one of the a-axes, have low visibility when imaged using diffraction vectors that are perpendicular to the stated a-axis.

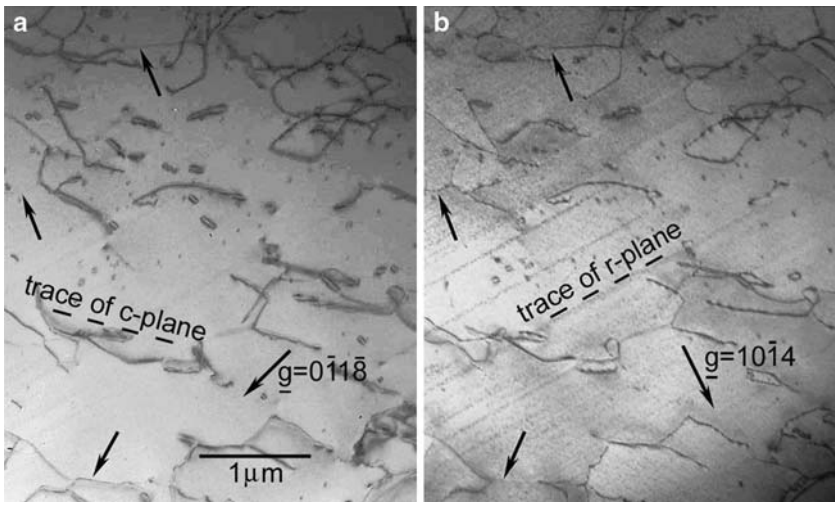

Fig. 4 TEM images showing loose networks formed by the interactions of dislocations produced by **c**-slip and **r**-slip. Part of a set of images that prove the existence of segments with $\langle\bar{2}110\rangle$Burgers vectors in the networks (note the *arrowed* segments with low visibility in image (**a**))

The diffraction contrast in Fig. 2 shows that the long dislocations are screws, which is consistent with their tendency to undergo climb at the test temperature (900 K) and thus develop a slightly helical character. The long screw dislocations occur in regions that have predominantly undergone basal slip in response to the torsional stresses applied to the specimen. The structure of calcite requires that the Burgers vector is the shortest translation vector in the basal plane, i.e., 1/3 $\langle\bar{2}110\rangle$, with a length of 4.99 Å.

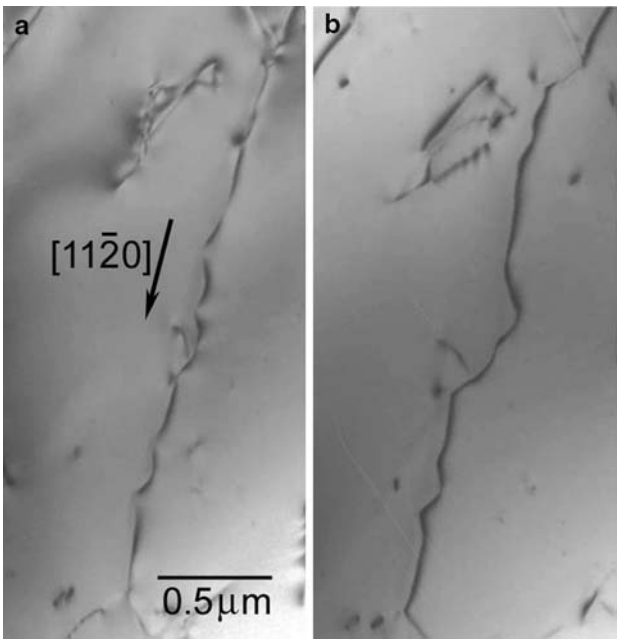

Fig. 5 TEM images of a basal screw dislocation that has started to cross-slip onto an **r**-plane. In image **a** the **r**-plane lies at a relatively small inclination to the electron beam and so the offset is not seen fully, whereas in image **b** the effect is obvious

Torsion experiments on calcite rock

Rybacki et al. (2003) investigated the rheology of synthetic calcite-quartz aggregates deformed to large strain in torsion and reported on their microstructural and mechanical characteristics. The experiments were conducted at constant twist rate under 400 MPa confining pressure and temperatures between 900 K and 1,300 K. Similar to earlier studies on Carrara marble by Pieri et al. (2001a, b) and Barnhoorn et al. (2004), ductile deformation was accompanied by dynamic recrystallization at large strains and high temperatures. Samples were originally 10 mm in length and 15 mm diameter. From the suite of samples we chose for this investigation one with minimal quartz content C1Q5 (99 wt.% calcite, 1 wt.% quartz). The aggregate with originally equiaxed 13 ± 3 μm grains, was deformed at 900 K and constant twist rate of 4.3×10^{-4} s^{-1} (corresponding to a shear strain rate of 3.2×10^{-4} s^{-1} at the sample periphery) to a maximum shear strain γ (at the surface) of about 5. During the experiment the sample weakened by a factor of about 1.6 from $\tau \approx 70$ MPa at $\gamma \approx 2$ to $\tau \approx 45$ MPa at $\gamma \approx 5$. Twist-rate steppings during deformation indicate a stress exponent of 4.5, used for the conversion from torque to shear stress data. Deformation produced highly flattened grains with aspect ratios exceeding 10:1. The long grain axes are oblique to the shear plane and indicate a dextral sense of shear (Fig. 6). As shown by Rybacki et al. (2003) penetrative recrystallization requires higher strains than $\gamma \approx 5$ under the experimental conditions. A qualitative assessment of thin sections with the petrographic microscope shows that the extremely strong shape preferred orientation does not correlate with the lattice preferred orientation, since individual crystallites have different extinctions.

Crystallographic preferred orientation (texture) was investigated with two methods: Electron back-scatter diffraction (EBSD) on a polished section and synchrotron hard X-ray diffraction on slabs in transmission. For EBSD a section was cut near the surface of the cylinder that experienced the largest amount of strain. Orientations were measured with the Berkeley Leo SEM-EBSD system in automatic mode (using a local system for microscope control and image acquisition and HKL software for pattern indexing) over an area of 1 × 3 mm with stepsize of 0.02 mm. From 3,760 indexed orientations with a mean angular deviation (MAD index) between observed and calculated diffraction bands of less than 1.0°, an orientation distribution (OD) was obtained in Beartex (Wenk et al. 1998) and, after smoothing with a 7.5° filter, from the OD some diagnostic pole figures were recalculated. Figure 7 illustrates a rather complex pattern, even for c-axes, indicating a wide range of orientations, with several orientation components. We show pole figures for $c = (0001), a = \{11\bar{2}0\}$ and $r = \{10\bar{1}4\}$. $\{10\bar{1}4\}$ is the cleavage rhomb and an important slip plane. With a maximum of 4.04 m.r.d. in (0001) pole figures the strength of preferred orientation is moderate and with a minimum of 0.18 m.r.d. a substantial number of grains are randomly oriented. Pole figures for $\{11\bar{2}0\}$ and $\{10\bar{1}4\}$ have much lower pole density variations than (0001).

To further explore texture variations we used synchrotron X-rays for spot analyses over a median section, 1 mm in thickness. The section was not exactly in the center and the deviation was corrected in the data analysis by applying corresponding rotations around the torsion axis. The advantage of synchrotron X-ray analysis is better statistics than EBSD by analyzing volume rather than surface, and the possibility to record texture changes across the sample. The general method has been described by Lonardelli et al. (2005). Experiments were conducted at beamline 11 ID-C of the Advanced Photon Source (APS) at Argonne National Laboratory with a 1 mm diameter beam of monochromatic X-rays (wavelength 0.108 Å). X-rays diffract on the irradiated sample volume and diffraction images are recorded with a MAR345 (3450 × 3450 pixels) image plate positioned 176 cm behind the sample. Five spots on the sample, with different distance from the cylinder axis, were measured to explore variations as function of shear strain (Fig. 8 bottom). For each spot three images were recorded at different tilt angles of the sample relative to the incident beam (–30°, 0°, 30°). Images were analyzed with the Rietveld method as implemented in MAUD (Lutterotti et al. 1999) and from the combination of three images the orientation distribution was obtained. Recalculated (0001) pole figures at five positions of the sample are shown in Fig. 8 (top).

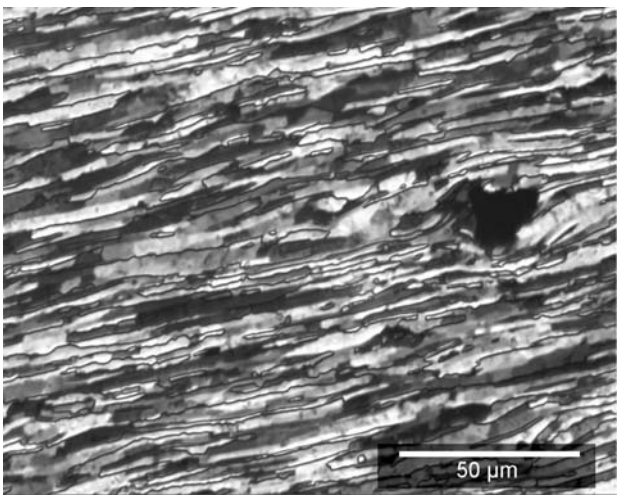

Fig. 6 Micrograph of sample C1Q5, twisted at 900 K to a shear strain of about 5. Crossed polars, length of long edge is 170 µm, shear sense is dextral. A single quartz grain is located at the right side of image (*black spot*)

Close to the surface of the sample spots 1 and 5 at about 13 mm diameter have the equivalent von Mises strain $\varepsilon_{eq} = 2.6$ ($\varepsilon_{eq} = \gamma/\sqrt{3}$ and $\gamma = D\,\Theta / 2L$, where D is diameter, Θ the twist angle and L the length). Pole figures on both sides are very similar, except that they are related by a vertical mirror plane since the sense of shear is reversed (Fig. 8, spots 1 and 5). This is best visible in the pole densities of subsidiary maxima. These (0001) pole figures also compare well with the EBSD pole figure (Fig. 7) with a similar maximum (spot 1 3.24 m.r.d. vs. 4.04 for EBSD) but a higher minimum (0.46 m.r.d. vs. 0.18 for EBSD). The X-ray texture is more reliable, particularly for the minimum, because of better statistics. A closer correspondence could be obtained by additional smoothing of the EBSD texture. There is not much change with radial distance. At spots 2 and 4 at a diameter of 6.5 mm (equivalent strain $\varepsilon_{eq} = 1.3$), pole figures are similar to those from near the surface, though somewhat more asymmetric (spot 4). Spot 2 may represent local sample heterogeneity. In the central part the (0001) pole figure has a single maximum that can be explained as an average around the torsion axis (Fig. 8, spot 3). Since the slab is about 1–2 mm removed ($\varepsilon_{eq} = 0.3$) from the center of the cylinder, strain is not negligible, but already at these small strains the texture is well developed (4.04 m.r.d. and 0.33 m.r.d.) The results indicate that at less than one half radial distance an essentially steady state was obtained, with no significant increase in strength with further shearing.

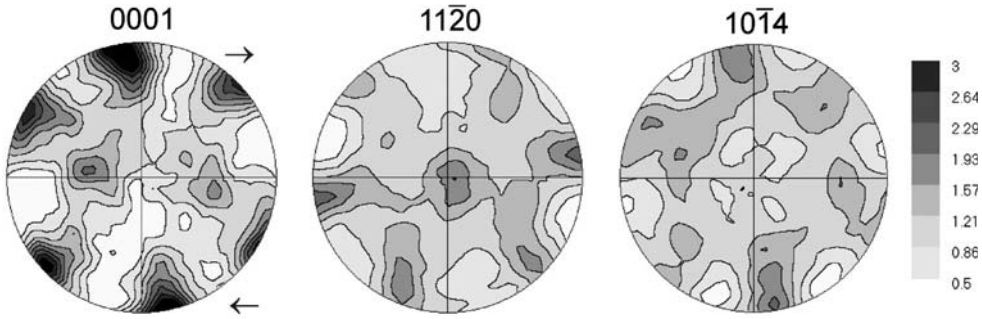

Fig. 7 Calcite pole figures for C1Q5 measured by EBSD. Shear plane horizontal, shear sense is indicated. Equal area projection, linear contour scale with pole densities in multiples of a random distribution (m.r.d.)

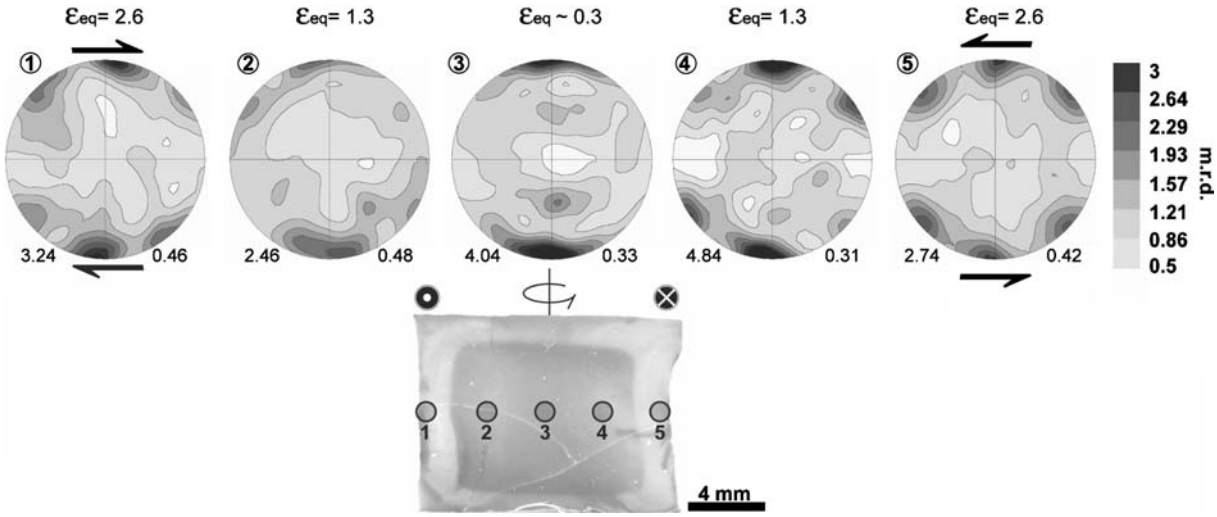

Fig. 8 (0001) pole figures measured with synchrotron X-rays in transmission across a median section of the sample. Maximum and minimum pole densities are indicated at the bottom of each pole figure and the equivalent von Mises strain ε_{eq} on top. Equal area projection, linear contour scale

Polycrystal plasticity simulations

Calcite has been the subject of pioneering studies not only on the experimental side, but also for texture simulations. It was one of the first minerals to which modern polycrystal plasticity theory was applied (Lister 1978). Texture transitions were attributed to different activities of slip systems, with mechanical twinning playing an important role at low temperature (Takeshita et al. 1987, Tomé et al. 1991). One problem with these simulations was that patterns predicted for high temperature were poorly matched by experiments. No simulations have been done for the new slip systems proposed by De Bresser and Spiers (1997) and a reevaluation is warranted.

The approach that we take is similar to the one described in detail by Tomé and Canova (2000) and known as visco-plastic polycrystal plasticity. It is based on a simplified assumption of individual grains, each deforming homogeneously and without interaction with neighbors. We assume an aggregate of 4,000 crystals, particular slip systems and critical resolved shear stresses, a hardening law (very weak work hardening was chosen, consistent with the experiment), and high strain rate sensitivity (stress exponent 4.5, Rybacki et al. 2003). Simple shear deformation is imposed in 50 increments to a total strain of $\varepsilon = 1$. Two types of conditions are explored. First simulations are done for homogeneous strain, deforming each grain the same amount (Taylor condition, Taylor 1938). This is consistent with the microstructure with all grains of similar shape, independent of orientation (Fig. 6). A second simulation is done for a viscoplastic self-consistent condition where each grain is embedded in an anisotropic homogeneous medium that represents the average over all orientations (Molinari et al. 1987). Here each grain has the freedom

to deform differently, depending on its orientation. For the simulations the Los Alamos viscoplastic self-consistent code VPSC6 was employed (Lebensohn and Tomé 1994). Numerous values for critical shear stresses (CRSS) were explored. We only show three sets (Table 1). Model A assumes slip systems and CRSS values corresponding closely to those suggested by De Bresser and Spiers (1997) with **r**, **f** and **c**-slip active. Model B is the same as A except that **r** = $\{10\bar{1}4\}\langle 11\bar{2}0\rangle$ has been added as a slip system. Model C is the same as A but **c**-slip is excluded.

Pole figures obtained from the simulated orientation distributions for the various models and conditions A, B and C are shown in Fig. 9a–d. A good match of experimental (Fig. 7) and simulated pole figures is obtained for model A with c-slip. Results are rather similar for Taylor (Fig. 9a) and self-consistent models (Fig. 9b), though $\{11\bar{2}0\}$ pole figures are rather weak. It is assumed that **c**-slip is slightly harder than **f**-slip. If **c**-slip is favored over **f**-slip (as implied by De Bresser and Spiers 1997) the fit becomes worse. Also better agreement is obtained if the negative sense for **r**-slip is slightly favored over the positive sense in accordance with the low temperature results of Turner et al. (1954) but different from suggestions of De Bresser and Spiers 1997). Results for model B, where $\{10\bar{1}4\}\langle 11\bar{2}0\rangle$ slip has been added, are similar as for model A (Fig. 9c) and based on texture patterns alone both combinations of slip systems are possible. In this case the $\{11\bar{2}0\}$ pole figure corresponds best with the experiment (Fig. 7). Without **c**-slip it is impossible to obtain a pattern that resembles the experiments, particularly the diagnostic (0001) pole figure with a maximum at high angles to the shear plane normal, displaced with the sense of shear (Fig. 9d).

For model A the average number of slip systems active in a grain is 6.0 for Taylor and 4.5 for the self-consistent model. Slip system activities at 50% strain are also indicated in Table 1. The dominant system is **r**-; **r**+ and **c**-slip are slightly less active and **f**-slip is subordinate if **c**-slip is allowed. Without **c**-slip, **f**-slip activity becomes significant (Model C).

Discussion

Transmission electron microscopy, as well as preferred orientation patterns, establish basal slip as an important slip system in calcite at high temperature. The finding of basal slip answers a long-standing puzzle about calcite: why dolomite should have $(0001)\langle 11\bar{2}0\rangle$ as a dominant slip mechanism, while it appeared to be lacking in calcite, which has a simpler crystal structure. Basal slip in calcite is unlikely at low temperature where mechanical **e**-twinning is dominant.

The difficulty of isolating basal slip in calcite is apparent from the need to set up special deformation experiments to demonstrate it under laboratory conditions. Except at high temperatures, the critical resolved shear stress for **c**-slip must be considerably greater than that for **r**-slip. This implies a high Peierl's stress opposing translation in the basal plane, which is borne out by the (initial) straightness of many of the observed screws. With single crystal torsion experiments we have now succeeded in unequivocally identifying $(0001)\langle 11\bar{2}0\rangle$ slip through direct observation of dislocation patterns.

Indications that climb has only slightly affected the observed dislocation configurations shows that the test temperature was below that required for recovery-controlled (power law) dislocation creep, which is limited by the slowest diffusing species of point defect (Barber 1990, p146). The evidence for some dislocations cross-slipping is probably significant. The overcoming of obstacles by this mechanism (together with dislocation glide, and minor shape-change-accommodating twinning) are probably the factors that govern creep of calcite at moderate temperatures, as conjectured by De Bresser and Spiers (1997).

Table 1 Slip systems, critical resolved shear stress coefficients (relative to **r**-) and slip system activities (in % at 50% strain)

	A			B		C	
	CRSS	Taylor	SC	CRSS	SC	CRSS	SC
r – $\{10\bar{1}4\}\langle 20\bar{2}\bar{1}\rangle$	1.0	31	33	1.0	28	1.0	19
r + $\{10\bar{1}4\}\langle\bar{2}021\rangle$	1.3	28	18	1.3	11	1.3	34
r$\{10\bar{1}4\}\langle\bar{1}2\bar{1}0\rangle$	4.5	2	0	1.5	26	4.5	3
f – $\{01\bar{1}2\}\langle 01\bar{1}\bar{1}\rangle$	1.5	7	10	1.5	8	1.5	15
f + $\{01\bar{1}2\}\langle 0\bar{1}11\rangle$	1.5	10	10	1.5	7	1.5	27
c$\{0001\}\langle 11\bar{2}0\rangle$	1.6	23	30	1.6	19	4.5	2
Average number of active slip systems		6.0	4.5		5.5		4.2

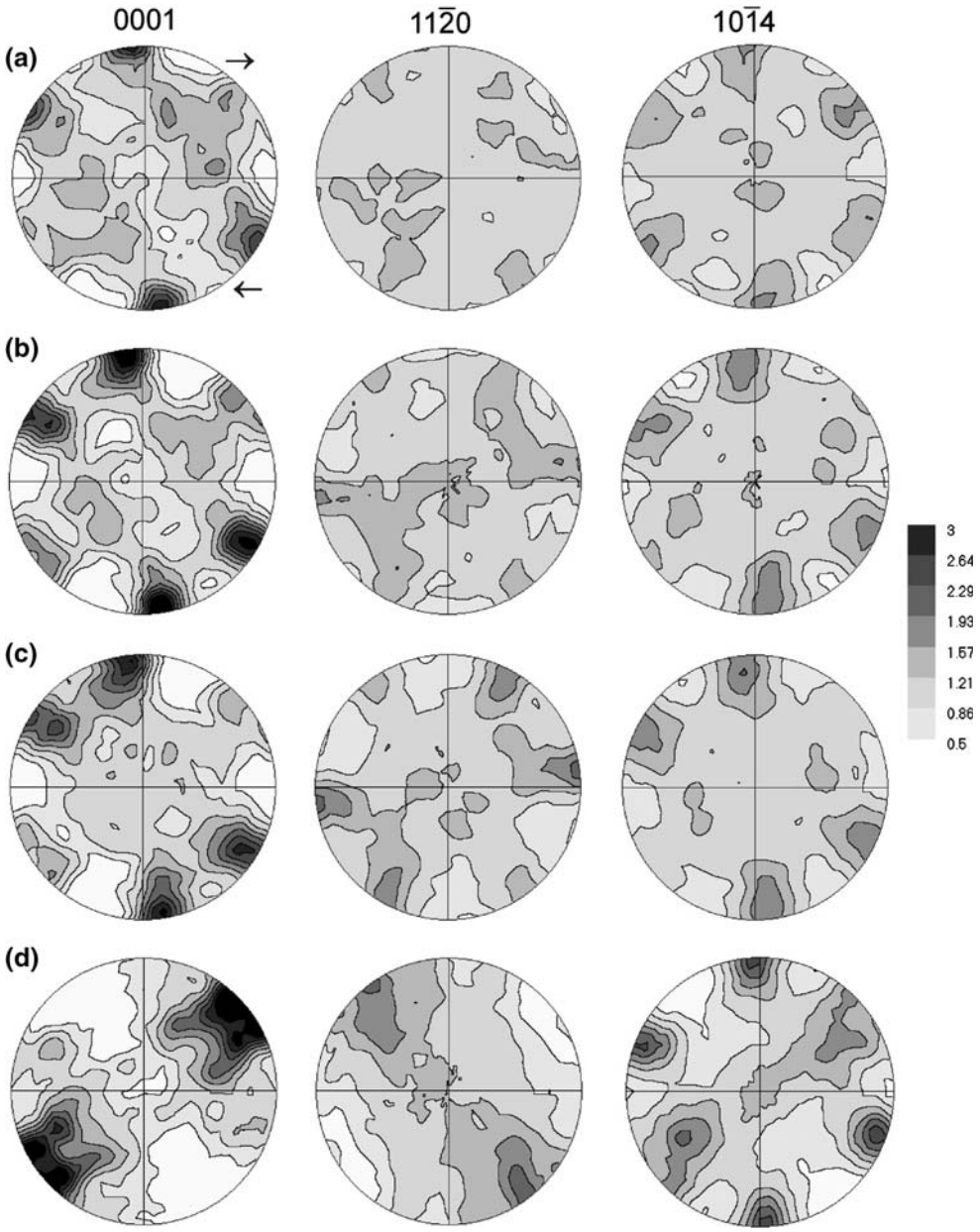

Fig. 9 Texture simulations for simple shear deformation of calcite. **a** Model A Taylor, **b** Model A self-consistent, **c** Model B self-consistent, **d** Model C self-consistent. Shear plane horizontal, shear sense is indicated (**a**). Equal area projection, linear contour scale with pole densities in m.r.d.

Observed textures need to be compared with other torsion experiments. The synthetic calcite-quartz rock textures are similar to those for Carrara marble reported by Pieri et al. (2001b) and Barnhoorn et al. (2004), but very different for Solnhofen limestone (Casey et al. 1998). In the latter case at 750°C = 1023 K, grains remained fairly equiaxed and c-axes concentrate in a broad maximum. Probably deformation mechanisms were different and grain-size sensitive creep and grain boundary sliding may have occurred.

The case of high temperature calcite torsion textures deserves a discussion of crystal rotations during simple shear deformation with implications about the sense of rotation of texture components, and about the intuitive contention that slip planes orient in the shear plane and slip directions in the shear direction (e.g., Etchecopar 1977). We have to distinguish rotations of the crystal shape and rotations of the crystal coordinate system relative to the shear plane. In the case of the calcite aggregate studied in this paper, deformation has been fairly homogeneous, crystallites becoming elongated and the long axis rotating towards the shear direction (Fig. 6). The crystallographic rotations due to slip are much more complex and this is best illustrated with rotation trajectories of selected orientations in c-axis pole figures for model A (Fig. 10). The symbol size is proportional to the grain deformation, thus the smallest symbol signifies the starting orientation. Both,

for Taylor (Fig. 10a) and self-consistent assumptions (Fig. 10b) c-axes of most orientations undergo large rotations, some in the sense of shear and others against the sense of shear. Some orientations, one with the c-axis close to the shear plane normal, barely rotate at all. There are only minor differences in the rotation trajectories between the Taylor and self-consistent model. The crystal rotations are generally larger than the grain shape rotation and much more irregular. There is no intuition guiding us to predict these rotations, since many slip systems (4.5 on average, even for self-consistent conditions) are involved in each crystal.

As is clear, rotations do not converge towards a single orientation, e.g., one with the slip plane in the shear plane and the slip direction in the shear direction, as is supported by the complex experimental texture pattern with three main maxima for c-axes. This is analogous to cubic face-centered metals with the only slip system $\{111\}\langle 1\bar{1}0\rangle$ and no concentration of $\{111\}$ poles in the shear plane normal, nor $\langle 1\bar{1}0\rangle$ poles in the shear direction (Hughes et al. 2000). In low symmetry materials with few slip systems such as triclinic plagioclase or orthorhombic olivine, intuitive interpretations may be more applicable. In simple shear the texture maxima that evolve are not a stable component but a temporary average of orientations where rotation gradients are slowest. This also can explain why textures do not become exceedingly strong, even at large strains. Rotations reach a steady state with some orientations moving into a maximum and others moving out of it.

Having discussed torsion textures we should return to the high temperature compression textures (Wenk et al. 1973) that could never be satisfactorily explained. A Taylor simulation for slip systems of model A and axial compression of 25% strain produces the inverse pole figure shown in Fig. 11a. The excellent comparison with the old experimental data is striking (Fig. 11b).

In conclusion we should comment on some implications for dynamic recrystallization. Dynamic recrystallization occurs at the highest temperatures and large strains, both in torsion experiments of calcite quartz rocks and Carrara marble (Barnhoorn et al. 2004; Pieri et al. 2001a, b; Rybacki et al. 2003). In this study we have selected a sample without recrystallization. As was pointed out by Pieri et al. (2001b) the strong recrystallization texture with two symmetrical components could either be explained as growth of hard orientations, using the conventional slip systems in Table 1, or as nucleation on very highly deformed grains, which would require $\mathbf{r} = \{10\bar{1}4\}\langle\bar{1}2\bar{1}0\rangle$ slip to be active. So far, there has been no experimental evidence for this slip system, though, like basal slip, this is also a common slip system in dolomite (Barber and Wenk 2001). We have done simulations that include $\{\mathbf{r}\}\langle a\rangle$ slip (Fig. 9c) and results are quite similar to those obtained without this system (Fig. 9b). Having established $\langle 11\bar{2}0\rangle$ as a slip direction and the existence of screw dislocations for basal slip, it is possible for these dislocations to cross-slip onto rhombohedral planes (unlike edge dislocations, screws are not restricted to the slip plane in which they formed). The dislocations that are strongly zig-zagged seem to be good evidence for this. When viewed down $\langle 10\bar{1}0\rangle$ they look fairly straight, but when tilted strongly one sees that they have segments that have moved out of the basal plane. Such dislocations are free to interact with dislocations generated by **r**-slip or slip on other rhombohedral planes, and thus can become incorporated into networks. Good evidence for this is the structure at Q' and Q'' in Fig. 3. It should be pointed out, however, that the presence of segments with $\langle 11\bar{2}0\rangle$ type Burgers vectors in a network does not necessarily imply the effects of basal slip because a $1/3\langle 11\bar{2}0\rangle$ Burgers vector can result from the interaction of two $1/6\langle 2\bar{2}01\rangle$ dislocations created by duplex **r**-slip (see Barber and Wenk 2001, Fig. 2b). Such interactions, rather than

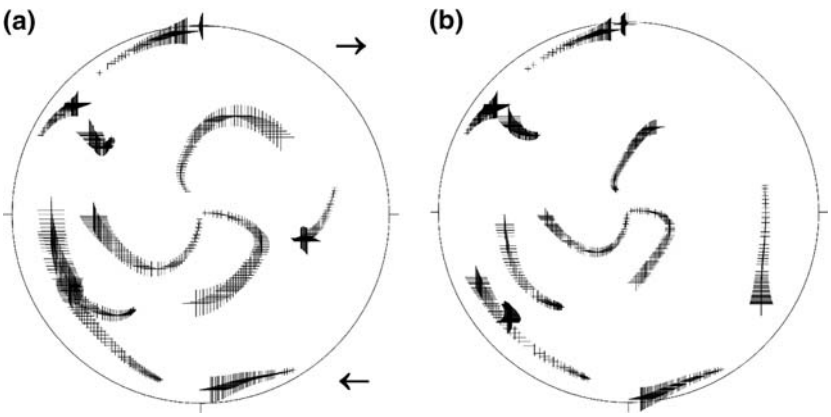

Fig. 10 (0001) Rotation trajectories of selected orientations during simple shear deformation. Shear plane is horizontal and shear sense is indicated. Symbol size is proportional to strain, i.e., the starting orientation is with the smallest symbol of each trail. **a** Taylor model, **b** self-consistent model. Equal area projection

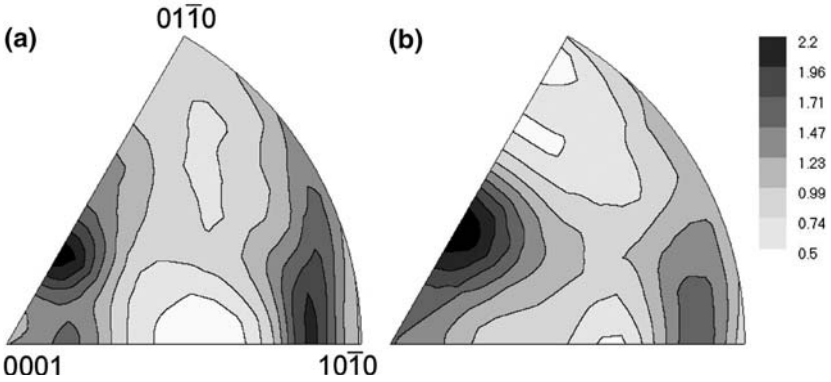

Fig. 11 Inverse pole figure for calcite deformed in compression. **a** Taylor simulation using slip systems for model A in Table 1 (including basal slip), 25% equivalent strain. **b** Experimentally deformed limestone at 973 K (sample VW31 from Wenk et al. 1973). Equal area projection, linear contours

cross-slip, may be the correct interpretation for the ⟨a⟩ segments imaged in Fig. 2. Based on these findings it is plausible that rhombohedral ⟨a⟩ slip is active at high temperature and may be responsible for the observed recrystallization textures (Pieri et al. 2001b).

Having established new high temperature slip systems with single crystal experiments (De Bresser and Spiers 1997), new single crystal torsion experiments and transmission electron microscopy show that calcite is more similar to dolomite than previously conceived. Taking these results into account we can now model compression and torsion textures satisfactorily and may even be closer to interpreting recrystallization. The long-standing calcite enigma seems to be resolved.

Acknowledgments We are appreciative to M. Naumann, S. Gehrmann and K. Peach for help with deformation experiments and sample preparation. Texture measurements were performed at beamline 11 ID of the Advanced Photon Source at Argonne with help by Y. Ren. We also thank J. Silver for access to the electron microscope. Reviews by Karsten Kunze and Chris Spiers were very helpful indeed. HRW is grateful for hospitality at the GeoForschungsZentrum Potsdam during a sabbatical leave. Research was supported by NSF (EAR 0337006) and DOE (DE-FG02-05ER15637), and a postdoctoral fellowship EX2005-0490MEC (JGB). The Humboldt Museum in Berlin kindly provided the calcite crystal used in this study.

References

Adams FD, Nicolson JT (1901) An experimental investigation into the flow of marble. R Soc Lond Philos Trans A 195:363–401

Barber DJ (1990) Regimes of plastic deformation—processes and microstructures: an overview. In: Barber DJ, Meredith PG (eds) Deformation processes in minerals, ceramics and rocks. Unwin Hyman, London

Barber DJ, Wenk H-R (2001) Dislocation behaviour in dolomite. Europ J Mineral 13:221–243

Barber DJ, Heard HC, Wenk H-R (1981) Experimental deformation of dolomite crystals from 20–800°C. Phys Chem Minerals 7:271–286

Barnhoorn A, Bystricky M, Burlini L, Kunze K (2004) The role of recrystallisation on the deformation behaviour of calcite rocks: large strain torsion experiments on Carrara marble. J Struct Geol 26:885–903

Barrett C, Massalski TB (1980) Structure of metals. 3rd revised edn. Pergamon Press, Oxford, p 395

Baumhauer H (1879) Ueber künstliche Kalkspath-Zwillinge nach ½ R. Z Kristall 3:588–591

Borg I, Handin J (1967) Torsion of calcite single crystals. J Geophys Res 72:641–669

Burlini L, Marquer D, Challandes N, Mazzola S, Zangarini N (1998) Seismic properties of highly strained marbles from the Spluegenpass, Central Alps. J Struct Geol 20:277–292

Casey M, Kunze K, Olgaards DL (1998) Texture of Solnhofen limestone deformed to high strains in torsion. J Struct Geol 20:255–267

De Bresser JHP, Spiers CJ. (1997) Strength characteristics of the r, f, and c slip systems in calcite. Tectonophysics 272:1–23

Dietrich D, Song H (1984) Calcite fabrics in a natural shear environment; the Helvetic nappes of western Switzerland. J Struct Geol 6:19–32

Dove HW (1860) Optische Notizen. Ann Phys 110:286–290

Erskine BG, Heidelbach F, Wenk H-R (1993) Lattice preferred orientations and microstructures of deformed Cordilleran marbles: correlation of shear indicators and determination of strain path. J Struct Geol 15:1189–1205

Etchecopar A (1977) A plane kinematic model of progressive deformation in a polycrystalline aggregate. Tectonophysics 39:121–139

Griggs DT, Turner FJ, Borg I, Sosoka J (1953) Deformation of Yule marble, Part V. Effects at 300°C. Geol Soc Am Bull 64:1327–1325

Hirsch PB, Howie A, Nicholson RB, Pashley DW, Whelan MJ (1965) Electron microscopy of thin crystals. Butterworths, London

Hughes DA, Lebensohn R, Wenk H-R, Kumar A (2000) Stacking fault energy and microstructure effects on torsion texture evolution. Proc R Soc Lond A 456:1–33

Jamison WR, Spang JH (1976) Use of calcite twin lamellae to infer differential stress. Geol Soc Am Bull 87:868–872

Johnsen A (1902) Biegungen und Translationen. N Jb Mineral Geol Palaeontol 133–153

Kern H, Wenk H-R (1983) Calcite texture development in experimentally induced ductile shear zones. Contrib Mineral Petrol 83:231–236

Lacombe O, Laurent P (1992) Determination of principal stress magnitudes using calcite twins and rock mechanics data. Tectonophysics 202:83–93

Lebensohn RA, Tomé CN (1994) A self-consistent visco-plastic model: prediction of rolling textures of anisotropic polycrystals. Mater Sci Eng A175:71–82

Lister GS (1978) Texture transitions in plastically deformed calcite rocks. Proceedings of the 5th international confer-

ence on texture of materials, Aachen. Springer, Berlin Heidelberg New York, pp 199–210
Lonardelli I, Wenk H-R, Lutterotti L, Goodwin M (2005) Texture analysis from synchrotron diffraction images with the Rietveld method: dinosaur tendon and salmon scale. J Synchr Radiation 12:354–360
Lutterotti L, Matthies S, Wenk H-R (1999) MAUD: a friendly Java program for materials analysis using diffraction. Int Union Crystallogr Comm Powder Diffraction Newsl 21:14–15
Molinari A, Canova GR, Ahzi S (1987) A self-consistent approach of the large deformation polycrystal viscoplasticity. Acta Metall 35:2983–2994
Muegge O (1898) Ueber Translationen und verwandte Erscheinungen in Krystallen: N. Jb Mineral Geol Palaeont 71–158
Paterson MS, Olgaard DL (2000) Rock deformation tests to large shear strains in torsion. J Struct Geol 22:1341–1358
Pieri M, Burlini L, Kunze K, Stretton I, Olgaard D (2001a) Rheological and microstructural evolution of Carrara marble with high shear strain: Results from high temperature torsion experiments. J Struct Geol 23:1393–1413
Pieri M, Kunze K, Burlini L, Strettom I, Olgaard D, Burg JP, Wenk H-R (2001b) Texture development of calcite by deformation and dynamic recrystallization at 1000 K during torsion experiments of marble to large strains. Tectonophysics 330:119–140
Ratschbacher L, Wenk H-R, Sintubin M (1991) Calcite textures: examples from nappes with strain-path partitioning. J Struct Geol 13:369–384
Rowe KJ, Rutter EH (1990) Paleostress estimation using calcite twinning: experimental calibration and application to nature. J Struct Geol 12:1–17
Rutter EH, Casey M, Burlini L (1994) Preferred crystallographic orientation development during the plastic and superplastic flow of calcite rocks. J Struct Geol 16:1431–1446
Rybacki E, Paterson M, Wirth R, Dresen G (2003) Rheology of calcite-quartz aggregates deformed to large strain in torsion. J Geophys Res 108:2089, DOI:10.1029/2002JB001833
Schmid SM, Casey M, Starkey J (1981) The microfabric of calcite tectonites from the Helvetic nappes (Swiss Alps). Geol Soc Lond Spec Publ 9:151–158
Schmid S, Panazzo R, Bauer S (1987) Simple shear experiments on calcite rocks: Rheology and microfabric. J Struct Geol 9:747–778
Takeshita T, Tomé CN, Wenk H-R, Kocks UF (1987) Single crystal yield surface for trigonal lattices: application to texture transitions in calcite polycrystals. J Geophys Res B92:12917–12920
Taylor GI (1938) Plastic strain in metals. J Inst Met 62:307–324
Tomé CN, Canova GR (2000) Self-consistent modeling of heterogeneous plasticity, Chapter 11 In: Kocks UF, Tomé CN, Wenk H-R (eds) Texture and anisotropy. preferred orientations in polycrystals and their effect on materials properties, 2nd Paperback Edtn, Cambridge University Press, Cambridge, pp 466–510
Tomé CN, Wenk H-R, Canova GR, Kocks UF (1991) Simulations of texture development in calcite: comparison of polycrystal plasticity theories. J Geophys Res 96:11865–11875
Turner FJ, Griggs DT, Heard HC (1954) Experimental deformation of calcite crystals. Bull Geol Soc Am 65:883–934
Turner FJ, Griggs DT, Clark RH Dixon RH (1956) Deformation of Yule marble, part VII: development of oriented fabrics at 300°C–400°C. Geol Soc Am Bull 67:1259–1294
Wagner F, Wenk H-R, Kern H, Van Houtte P, Esling C (1982) Development of preferred orientation in plane strain deformed limestone: Experiment and theory. Contrib Mineral Petrol 80:132–139
Wenk H-R, Venkitasubramanyan CS, Baker DW, Turner FJ (1973) Preferred orientation in experimentally deformed limestone. Contrib Mineral Petrol 38:81–114
Wenk H-R, Kern H, Van Houtte P, Wagner F (1986) Heterogeneous strain in axial deformation of limestone, textural evidence. In: Hobbs BE, Heard HC (eds) Mineral and rock deformation: laboratory studies. Am Geoph U Geophys Monogr 36:287–295
Wenk H-R, Matthies S, Donovan J, Chateigner D (1998) BEARTEX, a Windows-based program system for quantitative texture analysis. J Appl Cryst 31:262–269